Available online at www.sciencedirect.com
SCIENCE DIRECT®
Journal of Sound and Vibration 272 (2004) 937–965
JOURNAL OF SOUND AND VIBRATION
www.elsevier.com/locate/jsvi

A theoretical model for ground vibration from trains generated by vertical track irregularities

X. Sheng[a,1], C.J.C. Jones[b,*], D.J. Thompson[b]

[a] *Civil Engineering Department, East China Jiaotong University, Nanchang, Jiangxi 330013, People's Republic of China*
[b] *Institute of Sound and Vibration Research, University of Southampton, Southampton SO17 1BJ, UK*

Received 11 December 2001; accepted 9 April 2003

Abstract

A model is developed for predicting ground vibrations due to vertical track irregularities. This model incorporates vehicles, a track and a layered ground, and uses the moving axle loads and the vertical rail irregularities as its inputs. Outputs include the dynamic wheel–rail forces and the displacement power spectra of the track and the ground surface. Results from this model are presented for a single-axle vehicle model and a British Mark 3 passenger coach running on different tracks (a 'lighter ballasted track', a 'heavier ballasted track' and a slab track) at different speeds (25, 60 and 83 m/s). Based on these results, the effects of track structure, vehicle speed and frequency range on the observed vibration levels are identified. The different roles of the moving axle loads and the roughness-induced dynamic loads are indicated, at different frequencies and for train speeds below and above the lowest ground wave speed.

1. Introduction

The problem of ground vibrations generated by surface trains has received increased attention in the past few years and a number of theoretical models have been reported for predicting ground vibration from trains e.g., [1–3]. The new interest lies particularly in high-speed lines where train speeds may exceed the propagation velocities of the waves in the ground. Thus, most of the models only take into account the vibration generated by moving axle loads (also termed quasi-static loads), which, when moving at speeds in excess of ground or embankment structure wave speeds, directly excite propagating waves of the track/ground structure. For environmental

*Corresponding author. Tel.: +44-23-8059-3224; fax: +44-23-8059-3190.
E-mail address: cjcj@isvr.soton.ac.uk (C.J.C. Jones).
[1] Currently on leave at ISVR, University of Southampton, England.

0022-460X/$ - see front matter © 2003 Elsevier Ltd. All rights reserved.
doi:10.1016/S0022-460X(03)00782-X

vibration, however, it is still the case that slow heavy axle-load traffic on conventional lines gives rise to the majority of complaints about vibration in line-side buildings. In this case, as has been demonstrated in Refs. [4,5], dynamic forces arising at rail–wheel contacts are equally important as, or more important than, the quasi-static loads.

In Ref. [6], a model has been developed by Sheng et al. for predicting ground vibration generated by a single harmonic load moving along a railway track. This model can be easily extended to include multiple moving harmonic loads of a single frequency by applying the superposition principle. As it stands, the model requires that the wheel–rail forces at each frequency are known in advance. For the moving, 'quasi-static' (i.e., non-oscillating) axle loads this is straightforward. However, it is already concluded in Ref. [4], that for the case reported there at least, dynamic wheel–rail forces are responsible for higher responses in the ground than the quasi-static loads and should be taken into consideration.

To calculate the vertical dynamic wheel–rail forces a vehicle dynamics model must be used. A number of vehicle dynamics models have been developed, e.g., Ref. [7]. The aims of such models are to analyze ride quality, hunting motion, curving etc., rather than ground vibration. For their purposes, however, the ground is modelled as a rigid or Winkler foundation and the track is often truncated into a finite length. As a result, waves, which actually propagate away along the track and into the ground, would be reflected into the 'finite system'. The effect of the presence of an elastic ground on the dynamic wheel–rail forces therefore cannot be estimated using such models.

In the present work, the dynamic wheel–rail forces are assumed to be generated from the irregular vertical profiles of the wheel and rail running surfaces. The rail irregularities might include dipped joints and corrugations as well as general undulation in the 'track top'. The wheel irregularities can be wheel flats, surface irregularities and wheel eccentricity. The variations in the vertical profiles of either surface (wheel and rail) introduce a relative displacement input to the system, as shown in Section 3. The process is assumed to be linear, so that for a given wavelength λ, a displacement input is generated at the passing frequency $f = c/\lambda$, where c denotes the train speed. For the frequency range of 5–80 Hz, of interest for the perception of ground vibration, and a train speed range of 36–250 km/h (10–70 m/s), the corresponding wavelengths of the vertical irregularity lie within the range 0.125–14 m (or wavenumber from 0.4 to 50 rad/m). For long wavelengths, the measurement of track geometry is a matter of routine railway engineering practice. In the wavelength range of 1–100 m, ORE C116 [8] gives the power spectral density of rail irregularities, showing that with increasing wavelength, the power spectral density increases very quickly. Dings and Dittrich [9] and others have measured short wavelengths, for the purposes of rolling noise research. The spectra of rail 'roughness' given by Dings and Dittrich for the wavelength range of 0.08–0.2 m approximately overlap with the track geometry data, thereby extending the range for which typical values are known. Ref. [10] also presents the power spectral density of rail irregularities in different European countries.

This paper, as its title suggests, is intended to investigate ground vibration generated by vertical rail irregularities. To carry out such an investigation, a model comprising three subsystems, i.e., vehicles, a track and a ground, is needed. Such a model is described in the present paper. The vehicles are represented as multiple rigid body systems and the vertical dynamics of the vehicles are coupled to the track–ground model presented in Ref. [6]. This model uses both the moving axle loads and the rail irregularities as its inputs.. In Section 2, the formulae for the receptances of the subsystems are derived. A Hertzian contact spring [11] is introduced between each wheelset

and the rails. Compatibility of displacements at wheel–rail contact points couple the vehicles and the track–ground subsystem, and yield equations for the dynamic wheel–rail forces. The detail of this is presented in Section 3. Section 4 derives the relationship between the displacement (velocity and acceleration) power spectrum of the ground surface and the power spectral density of the vertical profile of the rails. Results from the model are presented in Section 5, in which the effects of train speed, track type and the layered structure of the ground are examined.

In considering the dynamic loads to be generated from the irregular profile of the running surfaces, the model neglects other mechanisms which may be put forward as possible sources of vibration. The model does not specifically include vibration generated because of varying support stiffness along the track. This may be due to variations in the ground or ballast stiffness. There is also a small difference in stiffness when a wheel load is situated over a sleeper compared to when it is between sleepers. Some of these effects might be partially accounted for in the current scheme if the undulations of the track are measured under an axle load. In Ref. [2] the sleepers are considered to provide discrete loads to the ground with a time, and therefore phase, difference corresponding to the sleeper spacing and the train speed. Here, the axle loads are considered to be distributed through the ballast and possible embankment, so that the wheel loading function applying to the ground interface is smooth. This assumption is inherent in the treatment of the track as having continuous distributed stiffness and mass. A separate paper is in preparation that will present a comparison between the model described here and measurements for three sites [5]. The comparison shows a good correspondence between the predictions and the measurements which include passenger stock travelling below and above the lowest wave speed in the ground and slow moving two-axle freight wagons. Justification for the neglect of some possible source mechanisms in the present work rests in the fact that generally the two mechanisms that are considered are successful in accounting for the level of vibration observed across the relevant range of frequency in these cases.

2. Receptances of the vehicle and the track–ground system

In this section, the receptances of a vehicle and a track–ground system are derived. For the frequency range of interest, the vehicle is modelled as a multiple-body system. The vehicle equations are given in the appendix. A rigid body, e.g., the car body in the vehicle, may have six degrees of freedom, accounting for three displacements of the mass centre and three rotations around three orthogonal axes. As only the vertical (in the xz plane where z is vertically downwards and x is along the rail) dynamics of the vehicle are considered, then each body has only two degrees of freedom, i.e., the vertical displacement of its mass centre and its pitch motion. In practice, the suspensions in the vehicle may have non-linear behaviour. However, to enable analysis in the frequency domain, here, each non-linear suspension is linearized. As a result, the differential equation of motion for the vehicle is linear and of constant coefficients and is specified by a mass matrix $[\mathbf{M}_V]$ and a stiffness matrix $[\mathbf{K}_V]$. Damping is introduced and included in the stiffness matrix, thus the elements of the stiffness matrix may be complex and may be frequency dependent. The mass and stiffness matrices of several typical vehicles are presented in the appendix.

The vertical forces between the wheelsets and the rails are denoted, from the first wheelset of the first vehicle to the last wheelset of the last vehicle, by $\mathbf{P}_1(t), \mathbf{P}_2(t), \ldots, \mathbf{P}_M(t)$, where M is the number of the forces. As only vertical dynamics are included, the forces are not separated into their components on the two rails. At time $t = 0$, the longitudinal co-ordinates of these forces are denoted by $a_1, a_2, \ldots, a_M$. For each wheel–rail force, there are two components: one is a moving 'quasi-static' load, i.e., the moving axle load, and the other is a moving dynamic load. The responses to the axle loads are independent of vehicle dynamics in the frequency range of interest. Therefore only the dynamic wheel–rail forces are considered here and hereinafter, $\mathbf{P}_1(t), \mathbf{P}_2(t), \ldots, \mathbf{P}_M(t)$ refer to these dynamic forces. The vertical displacement of the rail is denoted by $w_R(x, t)$. For positions on the ground surface, the vertical (z-direction) displacement is denoted by $w_{10}(x, y, t)$.

2.1. Receptances of the vehicle at the wheelsets

The differential equation of motion of a single vehicle is given by

$$[\mathbf{M}_V]\{\ddot{\mathbf{z}}_V(t)\} + [\mathbf{K}_V]\{\mathbf{z}_V(t)\} = -[\mathbf{B}]\{\mathbf{P}(t)\}, \tag{1}$$

where $[\mathbf{M}_V]$ and $[\mathbf{K}_V]$ ('V' means vehicle) denote the mass and stiffness matrices of the vehicle (not including the Hertzian contact spring), $\{\mathbf{z}_V(t)\}$ the (generalized) displacement vector, $\{\mathbf{P}(t)\}$ the wheel–rail force vector and $[\mathbf{B}]$ is a matrix of unit and zero elements (see appendix). The minus sign before $\{\mathbf{P}(t)\}$ indicates that the positive wheel–rail forces are of compression of the contact spring.

To derive the receptances (displacements due to a unit force) of the vehicle at the wheelsets, let $\{\mathbf{P}(t)\} = \{\tilde{\mathbf{P}}(\Omega)\}e^{i\Omega t}$ and $\{\mathbf{z}_V(t)\} = \{\tilde{\mathbf{z}}_V(\Omega)\}e^{i\Omega t}$, where Ω denotes the angular frequency. Then Eq. (1) yields

$$\{\tilde{\mathbf{z}}_V(\Omega)\} = -([\mathbf{K}_V] - \Omega^2[\mathbf{M}_V])^{-1}[\mathbf{B}]\{\tilde{\mathbf{P}}(\Omega)\} = -[\mathbf{\Sigma}_V]\{\tilde{\mathbf{P}}(\Omega)\}, \tag{2}$$

where

$$[\mathbf{\Sigma}_V] = ([\mathbf{K}_V] - \Omega^2[\mathbf{M}_V])^{-1}[\mathbf{B}]. \tag{3}$$

The receptance between the jth and the kth wheelsets within a vehicle is denoted by σ_{jk}^W ('W' means wheelset), where, $j, k = 1, 2, \ldots, N$; N being the number of the wheelsets of the vehicle. In other words, σ_{jk}^W denotes the displacement amplitude of the jth wheelset due to a unit vertical harmonic load of frequency Ω exerted at the kth wheelset. These are a subset of the matrix $[\mathbf{\Sigma}_V]$. Thus the complex amplitudes of the displacements of the wheelsets produced by the wheel–rail forces are given by

$$\{\tilde{\mathbf{z}}_W(\Omega)\} = -[\mathbf{\Sigma}_W]\{\tilde{\mathbf{P}}(\Omega)\}, \tag{4}$$

where

$$[\mathbf{\Sigma}_W] = (\sigma_{jk}^W)_{j,k=1,2,\ldots,N} = \begin{bmatrix} \sigma_{11}^W & \cdots & \sigma_{1N}^W \\ \vdots & \cdots & \vdots \\ \sigma_{N1}^W & \cdots & \sigma_{NN}^W \end{bmatrix} \tag{5}$$

the receptance matrix of the vehicle at the wheelsets denotes. This matrix is dependent on the vehicle parameters, Ω, and is symmetric

$$\{\tilde{\mathbf{z}}_W(\Omega)\} = (\tilde{z}_{W1}(\Omega), \tilde{z}_{W2}(\Omega), \tilde{z}_{W3}(\Omega), \ldots, \tilde{z}_{WN}(\Omega))^{\mathrm{T}} \tag{6}$$

is the displacement vector of the wheelsets of the vehicle, and

$$\{\tilde{\mathbf{P}}(\Omega)\} = (\tilde{P}_1(\Omega), \tilde{P}_2(\Omega), \tilde{P}_3(\Omega), \ldots, \tilde{P}_N(\Omega))^{\mathrm{T}} \tag{7}$$

is the force vector exerted at the wheelsets by the rails. (Note: when referring to a train, $\{\tilde{\mathbf{P}}(\Omega)\}$ denotes the wheel–rail contact force vector of the whole train.)

The displacement vector of the wheelsets forms part of that of the corresponding vehicle. Therefore, it may be written that

$$\{\tilde{\mathbf{z}}_W(\Omega)\} = [\mathbf{A}]\{\tilde{\mathbf{z}}_V(\Omega)\}, \tag{8}$$

where $[\mathbf{A}]$ is a constant matrix and $[\mathbf{A}] = [\mathbf{B}]^{\mathrm{T}}$ (see the appendix). Thus Eqs. (3) and (4) give

$$[\mathbf{\Sigma}_W] = [\mathbf{A}][\mathbf{\Sigma}_V] = [\mathbf{A}]([\mathbf{K}_V] - \Omega^2[\mathbf{M}_V])^{-1}[\mathbf{B}]. \tag{9}$$

Eq. (9) gives the receptance matrix at the wheelsets for a single vehicle. Suppose there are N_1 identical vehicles being considered, then the total number of the wheel–rail forces is $M = N_1 N$. Assuming that the vehicles are coupled only by the rails, then the receptance matrix at the wheelsets for the train, denoted by $[\mathbf{\Sigma}_T]$ ('T' means train), is given by

$$[\mathbf{\Sigma}_T] = \mathrm{diag}([\mathbf{\Sigma}_W], \ldots, [\mathbf{\Sigma}_W]) = \begin{bmatrix} [\mathbf{\Sigma}_W] & \cdots & 0 \\ \vdots & \vdots & \vdots \\ 0 & \cdots & [\mathbf{\Sigma}_W] \end{bmatrix}. \tag{10}$$

The elements of matrix $[\mathbf{\Sigma}_T]$ are denoted by σ_{lk}^T, where, $k, l = 1, 2, \ldots, M$.

2.2. Receptances of the track–ground system at the wheel–rail contact points

The track–ground model described in detail in Ref. [6] used to calculate the receptances of the track–ground system is. In that model, the rail supports are modelled using continuous properties. Any effect of the discrete supports of the rails at sleeper positions is therefore not included. Suppose a unit vertical harmonic load $\mathrm{e}^{\mathrm{i}\Omega t}$, which is pointing downwards and located at $x = 0$ when $t = 0$, moves at speed c along the rails. As has been shown in Ref. [6], the steady state displacements of the rails and the ground surface (vertical component) are given by

$$\begin{aligned} w_R(x, t) &= w_R^{\Omega}(x - ct)\mathrm{e}^{\mathrm{i}\Omega t}, \\ w_{10}(x, y, t) &= w_{10}^{\Omega}(x - ct, y)\mathrm{e}^{\mathrm{i}\Omega t}. \end{aligned} \tag{11}$$

Eq. (11) means that, observed in a reference frame moving with the load at speed c, the displacements of the track–ground system are harmonic and have the same frequency as the load. Thus, the receptance at the jth wheel–rail contact point due to a unit load at the kth wheel–rail contact point (both of the points are moving at speed c) on the rail is determined by

$$\sigma_{jk}^R = w_R^{\Omega}(l_{jk}), \tag{12}$$

where

$$l_{jk} = a_j - a_k \tag{13}$$

is the distance between the two contact points, and when the jth contact point is ahead of the kth contact point, $l_{jk} > 0$.

The complex amplitudes of the displacements at the wheel–rail contact points on the rails are given by

$$\{\tilde{\mathbf{z}}_R(\Omega)\} = [\mathbf{\Sigma}_R]\{\tilde{\mathbf{P}}(\Omega)\}, \tag{14}$$

where

$$[\mathbf{\Sigma}_R] = \begin{bmatrix} \sigma_{11}^R & \sigma_{12}^R & \cdots & \sigma_{1M}^R \\ \sigma_{21}^R & \sigma_{22}^R & \cdots & \sigma_{2M}^R \\ \vdots & \vdots & \vdots & \vdots \\ \sigma_{M1}^R & \sigma_{M2}^R & \cdots & \sigma_{MM}^R \end{bmatrix} \tag{15}$$

the receptance matrix of the track–ground system at the wheel–rail contact points is. Notice that when the train speed is non-zero, this matrix is non-symmetric due to the load motion.

$$\{\tilde{\mathbf{z}}_R(\Omega)\} = (\tilde{z}_{R1}(\Omega), \tilde{z}_{R2}(\Omega), \tilde{z}_{R3}(\Omega), \tilde{z}_{RM}(\Omega))^{\mathrm{T}} \tag{16}$$

represents the displacement vector of the rail at the wheel–rail contact points observed in the moving frame of reference.

3. Coupling of the vehicles and the track–ground system

The vertical profile of the rail may be decomposed into a spectrum of discrete harmonic components. A single harmonic component is denoted by $z(x) = A\mathrm{e}^{\mathrm{i}(2\pi/\lambda)x} = A\mathrm{e}^{\mathrm{i}\beta x}$, where λ denotes the wavelength and A the amplitude which may be complex. At the moment t, the lth wheelset arrives at $x = a_l + ct$, thus the displacement input at the lth wheel–rail contact point is

$$z_l(t) = \tilde{z}_l(\Omega)\mathrm{e}^{\mathrm{i}\Omega t} = A\mathrm{e}^{\mathrm{i}(2\pi/\lambda)(a_l+ct)} = A\mathrm{e}^{\mathrm{i}(2\pi/\lambda)a_l}\mathrm{e}^{\mathrm{i}2\pi(c/\lambda)t}, \tag{17}$$

where

$$\tilde{z}_l(\Omega) = A\mathrm{e}^{\mathrm{i}(2\pi/\lambda)a_l}, \quad \Omega = 2\pi c/\lambda = c\beta. \tag{18}$$

The coupling of a wheelset with the rails is illustrated in Fig. 1, where $\tilde{z}_{Wl}(\Omega)\mathrm{e}^{\mathrm{i}\Omega t}$ denotes the displacement of the lth wheelset. A Hertzian contact spring is inserted between the wheelset and the rails. The stiffness of the Hertzian contact spring is denoted by k_{Hl}. It is assumed that the wheelset is always in contact with the rails, thus

$$\tilde{z}_{Wl}(\Omega) = \tilde{z}_{Rl}(\Omega) + \tilde{z}_l(\Omega) + \tilde{P}_l(\Omega)/k_{Hl}. \tag{19}$$

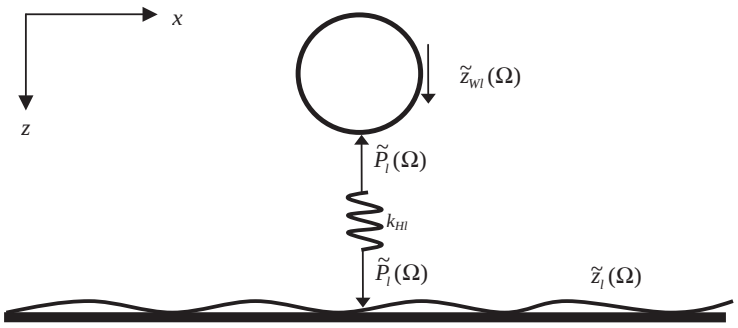

Fig. 1. Coupling of the lth wheelset with the rails.

From Eqs. (4) and (14)

$$\tilde{z}_{Wl}(\Omega) = -\sum_{k=1}^{M} \sigma_{lk}^{T} \tilde{P}_k(\Omega), \tag{20}$$

$$\tilde{z}_{Rl}(\Omega) = \sum_{k=1}^{M} \sigma_{lk}^{R} \tilde{P}_k(\Omega). \tag{21}$$

Inserting these two equations into Eq. (19) yields

$$\sum_{k=1}^{M} (\sigma_{lk}^{T} + \sigma_{lk}^{R}) \tilde{P}_k(\Omega) + \frac{1}{k_{Hl}} \tilde{P}_l(\Omega) = -\tilde{z}_l(\Omega) \quad (l = 1, 2, \ldots, M). \tag{22}$$

Eq. (22) is a set of linear algebraic equations with unknowns $\{\tilde{\mathbf{P}}(\Omega)\}$. When Eq. (22) is solved for $\{\tilde{\mathbf{P}}(\Omega)\}$, the displacements of the ground surface and of the rails at excitation frequency Ω are given by applying the superposition principle

$$\begin{aligned} w_R(x,t) &= \textstyle\sum_{l=1}^{M} w_R^{\Omega}(x - a_l - ct) \tilde{P}_l(\Omega) \mathrm{e}^{\mathrm{i}\Omega t}, \\ w_{10}(x,y,t) &= \textstyle\sum_{l=1}^{M} w_{10}^{\Omega}(x - a_l - ct, y) \tilde{P}_l(\Omega) \mathrm{e}^{\mathrm{i}\Omega t}. \end{aligned} \tag{23}$$

4. Response power spectra of the ground surface

4.1. Response to dynamic forces

Once the wheel–rail forces are obtained, the displacement spectra of the ground surface can be evaluated. In this section, formulae are derived for the response power spectra of the ground surface at a point that is stationary as the train moves past it. To do so, the vertical displacement spectrum of point (x, y) on the ground surface due to a unit amplitude rail irregularity of wavelength λ, $z(x) = \mathrm{e}^{\mathrm{i}(2\pi/\lambda)x} = \mathrm{e}^{\mathrm{i}\beta x}$, is denoted by $S_w^0(x, y, f; \Omega)$, where f is the frequency at which the spectrum is evaluated and Ω is the excitation angular frequency determined by

$$\Omega = 2\pi c/\lambda = c\beta \tag{24}$$

$S_w^0(x,y,f;\Omega)$ may be obtained by Fourier transforming Eq. (23) with respect to time t. A complete vertical rail profile made of a large number of discrete wavenumber components β_k, is described by the Fourier series

$$z(x) = \frac{1}{2\pi}\sum_{k=-\infty}^{\infty} \tilde{z}(\beta_k)\mathrm{e}^{\mathrm{i}\beta_k x}\Delta\beta, \tag{25}$$

where $\beta_k = k\Delta\beta$ and $\Delta\beta$ denotes the spacing of the discrete wavenumbers. With this input, the total displacement spectrum is given by

$$S_w(x,y,f) = \frac{\Delta\beta}{2\pi}\sum_{k=-\infty}^{\infty} S_w^0(x,y,f;\Omega_k)\tilde{z}(\beta_k), \tag{26}$$

where according to Eq. (24), $\Omega_k = c\beta_k$. Eq. (26) yields,

$$\begin{aligned}|S_w(x,y,f)|^2 &= \frac{(\Delta\beta)^2}{4\pi^2}\sum_{k=-\infty}^{\infty} S_w^0(x,y,f;\Omega_k)\tilde{z}_k \sum_{j=-\infty}^{\infty} S_w^{0*}(x,y,f;\Omega_j)\tilde{z}_j^* \\ &= \frac{(\Delta\beta)^2}{4\pi^2}\sum_{j=-\infty}^{\infty}\sum_{k=-\infty}^{\infty} S_w^0(x,y,f;\Omega_k)S_w^{0*}(x,y,f;\Omega_j)\tilde{z}_k\tilde{z}_j^*,\end{aligned} \tag{27}$$

where $\tilde{z}_j = \tilde{z}(\beta_j)$ and $\tilde{z}_j^*$ denotes the conjugate of $\tilde{z}_j$.

It is assumed that each harmonic component of the rail vertical profile is independent of the others, i.e.,

$$\mathrm{E}[\tilde{z}_k\tilde{z}_j^*] = \begin{cases} 0, & \text{if } k \neq j, \\ \mathrm{E}[|\tilde{z}_k|^2], & \text{if } k = j, \end{cases} \tag{28}$$

where E is the expected value operator. Thus Eq. (27) gives,

$$\mathrm{E}[|S_w(x,y,f)|^2] = \frac{(\Delta\beta)^2}{4\pi^2}\sum_{k=-\infty}^{\infty} |S_w^0(x,y,f;\Omega_k)|^2\mathrm{E}[|\tilde{z}_k|^2]. \tag{29}$$

The assumption made in Eq. (28), that the irregularity can be treated as a random function, is based on the idea that the irregularities of different wavelengths are due to different factors and those factors are independent of each other.

$\mathrm{E}[|S_w(x,y,f)|^2]$ gives the vertical displacement power spectrum of point (x,y) on the ground surface and is denoted by $P_w(x,y,f)$. Thus from Eq. (29)

$$\begin{aligned}P_w(x,y,f) &= \frac{L}{L}\frac{(\Delta\beta)^2}{4\pi^2}\sum_{k=-\infty}^{\infty} |S_w^0(x,y,f;\Omega_k)|^2\mathrm{E}[|\tilde{z}_k|^2] \\ &= \frac{(\Delta\beta)^2 L}{4\pi^2}\sum_{k=-\infty}^{\infty} |S_w^0(x,y,f;\Omega_k)|^2\frac{1}{L}\mathrm{E}[|\tilde{z}_k|^2],\end{aligned} \tag{30}$$

where L is a length over which the power spectral density (PSD), denoted by $P_z(\beta)$, of the vertical profile of the rails is estimated, and $\Delta\beta L = 2\pi$. It is known that $\frac{1}{L}\mathrm{E}[|\tilde{z}_k|^2] \approx P_z(\beta_k)$. Thus

$$P_w(x,y,f) = \frac{1}{2\pi}\sum_{k=-\infty}^{\infty} |S_w^0(x,y,f;\Omega_k)|^2 P_z(\beta_k)\Delta\beta. \tag{31}$$

Since the vertical profile of the rails, described by $z(x)$, is a real function of x, its power spectral density $P_z(\beta)$ is an even function of β. Therefore Eq. (30) can be written as

$$\begin{aligned} P_w(x,y,f) = &\frac{1}{2\pi}\sum_{k=1}^{\infty}[|S_w^0(x,y,f;\Omega_k)|^2 + |S_w^0(x,y,f;-\Omega_k)|^2]P_z(\beta_k)\Delta\beta \\ &+ \frac{1}{2\pi}|S_w^0(x,y,f;0)|^2 P_z(0)\Delta\beta. \end{aligned} \tag{32}$$

It can be shown that $S_w^0(x,y,-f;\Omega_k) = S_w^{0*}(x,y,f;-\Omega_k)$ which implies that $P_w(x,y,f)$ is an even function of frequency f. However, it should be noticed that, in general $S_w^0(x,y,f;\Omega_k) \neq S_w^{0*}(x,y,f;-\Omega_k)$.

In Eq. (32), the last term should be zero since it corresponds to an excitation of zero frequency at which, by definition, the dynamic wheel–rail contact forces vanish.

4.2. Addition of the quasi-static axle loads

Now the power spectrum due to the moving axle loads is added to Eq. (32) to give the total power spectrum. If $S_w^0(x,y,f;0)$ is now made to refer to the vertical displacement spectrum produced by the moving axle loads, then the associated power spectrum is $|S_w^0(x,y,f;0)|^2$. Thus the total power spectrum, also denoted by $P_w(x,y,f)$, is given by

$$\begin{aligned} P_w(x,y,f) = &\frac{1}{2\pi}\sum_{k=1}^{\infty}[|S_w^0(x,y,f;\Omega_k)|^2 + |S_w^0(x,y,f;-\Omega_k)|^2]P_z(\beta_k)\Delta\beta \\ &+ |S_w^0(x,y,f;0)|^2. \end{aligned} \tag{33}$$

Eq. (33) gives the relationship between the displacement power spectrum of the ground surface and the power spectral density of the vertical profile of the rails. Note that in Eq. (33) the displacement power spectrum is presented in units of $\mathrm{m}^2/(\mathrm{Hz})^2$ while the spectral density of the rail profile is in $\mathrm{m}^2/(\mathrm{cycle/m})$. It can be shown that $|S_w^0(x,y,f;\Omega_k)|^2$ is independent of x as well as the position of the train, and therefore the total power spectrum of the ground surface is also independent of x and the train position.

If all the wheelsets have the same power spectral density of vertical profile, then that power spectral density can be added to that of the rails. With the total power spectral density, Eq. (33) gives the displacement power spectrum of the ground surface due to the combined wheel–rail irregularities.

The velocity power spectrum, $P_{\dot{w}}(x,y,f)$, and the acceleration power spectrum, $P_{\ddot{w}}(x,y,f)$, of the ground surface are given by

$$P_{\dot{w}}(x,y,f) = (2\pi f)^2 P_w(x,y,f), \tag{34}$$

$$P_{\ddot{w}}(x,y,f) = (2\pi f)^2 P_{\dot{w}}(x,y,f) = (2\pi f)^4 P_w(x,y,f). \tag{35}$$

When divided by a chosen period of time, which normally is the time needed for a train to pass a fixed point, Eqs. (33)–(35) give the response power spectral density of the ground surface.

5. Results and discussion

5.1. Results for a single-axle vehicle model

In order to demonstrate some of the characteristics of the response of the system, a calculation is performed in this section for a single-axle vehicle model comprising a suspended mass M_C and an unsprung mass M_W. Each mass only has one degree of freedom in the vertical direction. The parameters for this vehicle model are deduced from the parameters of a freight wagon [7] are listed in Table 1. From Table 1 the axle load is 205.8 kN. The radius of the wheel is 0.42 m and the Hertz contact stiffness is estimated as 2.7×10^9 N/m (for two wheels). The natural frequency of the suspended mass on the suspension is evaluated as $\frac{1}{2\pi}\sqrt{k_{S1}/M_C} = 1.87$ Hz.

A layered ground specified by the parameters in Table 2 and two ballasted tracks specified by Table 3 (a lighter ballasted track) and Table 4 (a heavier ballasted track) are used in the calculation. The ground consists of a 2 m layer of material with a shear wave speed of 81 m/s (a Rayleigh wave speed of 77 m/s), overlying a half-space of stiffer material having a shear wave speed of 245 m/s. The characteristics associated with these ground and track parameters are discussed in detail in Refs. [6,12]. The calculation of the dispersion curves of the ground shows that from about 13 Hz, a second propagating mode with higher phase speed occurs in the layer [1]. This frequency is therefore sometimes termed a 'cut-on' frequency. The cut-on of the propagating mode leads to a rise in the frequency response of the ground between about 10 and 20 Hz.

A vertical irregular profile of the rail with an amplitude of 0.1 mm at all wavelengths is introduced as the excitation.

Table 1
Parameters for the single-axle vehicle model

Suspended mass (kg)	Unsprung mass (kg)	k_{S1} (N/m)	c_{s1} (Ns/m)	k'_{S1} (N/m)
19250	1750	2.66×10^6	3.5×10^4	3×10^6

Table 2
Parameters for a layered ground

Layer	Depth (m)	Young's modulus (10^6 N m^{-2})	Poisson ratio	Density (kg/m^3)	Loss factor	*P*-wave speed (m/s)	*S*-wave speed (m/s)	Rayleigh wave speed (m/s)
1	2.0	30	0.47	1550	0.1	340	81.1	77
Half-space		360	0.49	2000	0.1	1755	245	233

Table 3
Parameters for a lighter ballasted railway track

Mass of rail beam per unit length of track	120 kg/m
Bending stiffness of rail beam	1.26×10^7 N m^2
Loss factor of the rail	0.01
Rail pad stiffness	3.5×10^8 N/m^2
Rail pad loss factor	0.15
Mass of sleepers per unit length of track	490 kg/m
Mass of ballast per unit length of track	1200 kg/m
Ballast stiffness per unit length of track	3.15×10^8 N/m^2
Loss factor of ballast	1.0
Contact width of railway and ground	2.7 m

Table 4
Parameters for a heavier ballasted railway track

Mass of rail beam per unit length of track	120 kg/m
Bending stiffness of rail beam	1.26×10^7 N m^2
Loss factor of the rail	0.01
Rail pad stiffness	3.5×10^8 N/m^2
Rail pad loss factor	0.15
Mass of sleepers per unit length of track	490 kg/m
Mass of ballast per unit length of track	3300 kg/m
Ballast stiffness per unit length of track	1.775×10^8 N/m^2
Loss factor of ballast	1.0
Contact width of railway and ground	2.7 m

5.1.1. When the single axle runs on the lighter track on the ground

Fig. 2 shows the magnitude of the dynamic wheel–rail force plotted against excitation frequency (speed divided by wavelength) for three travelling speeds, 0, 30 m/s (108 km/h) and 60 m/s (216 km/h). Figs. 3 and 4 show the magnitudes of the displacements of the contact points on the wheel and on the rail.

Generally the magnitude of the wheel–rail force increases with frequency and achieves a broad maximum at around 80 Hz. As the travelling speed increases, this frequency decreases slightly and the maximum wheel–rail force decreases. The wheel–rail force is often calculated without considering the vehicle motion since, as indicated here, the effect of the vehicle motion is negligible for low frequencies and low vehicle speeds.

Within the overall shape of the spectrum of the contact force and the wheel and rail displacements, a couple of features can be identified that are associated with the resonance of the vehicle suspension. As can be seen, Figs. 2 and 4 indicate a very small peak at 2 Hz, while Fig. 3 shows a local minimum at this frequency. This frequency is close to the natural frequency of the suspended mass on the suspension.

Now in Eq. (22) let $M = 1$, so that

$$\tilde{P}_1(\Omega) = -\frac{\tilde{z}_1(\Omega)}{(\sigma_{11}^T + \sigma_{11}^R + 1/k_{H1})}, \tag{36}$$

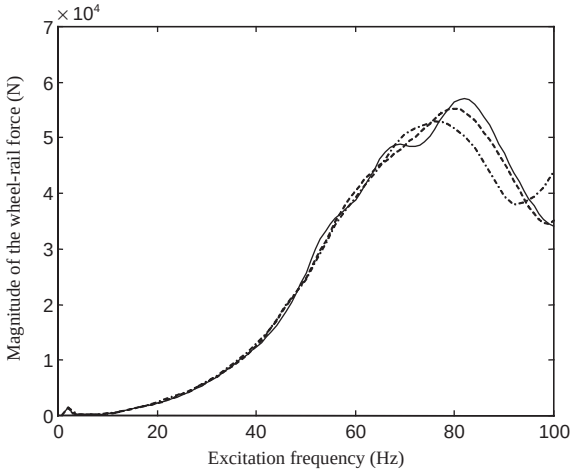

Fig. 2. Magnitude of the wheel–rail force for the single-axle model plotted against frequency of excitation for an irregularity of amplitude 0.1 mm. ——, for vehicle running at 0 m/s; – – –, for vehicle running at 30 m/s; –·–, for vehicle running at 60 m/s.

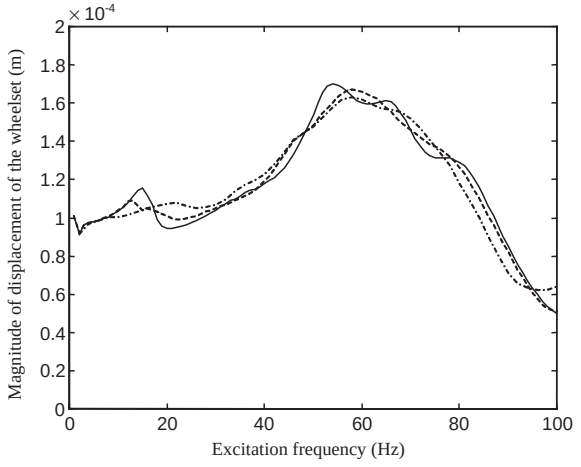

Fig. 3. Magnitude of the displacement of the wheelset for the single-axle model plotted against frequency of excitation for irregularity of amplitude 0.1 mm. ——, for vehicle running at 0 m/s; – – –, for vehicle running at 30 m/s; –·–, for vehicle running at 60 m/s.

where σ_{11}^R denotes the receptance of the rail at the wheel–rail contact point, σ_{11}^T the receptance of the vehicle at the wheelset, given by

$$\sigma_{11}^T = \frac{1-(\Omega/\omega_0)^2}{\omega_0^2(\Omega/\omega_0)^2[M_W(\Omega/\omega_0)^2-(M_C+M_W)]}, \tag{37}$$

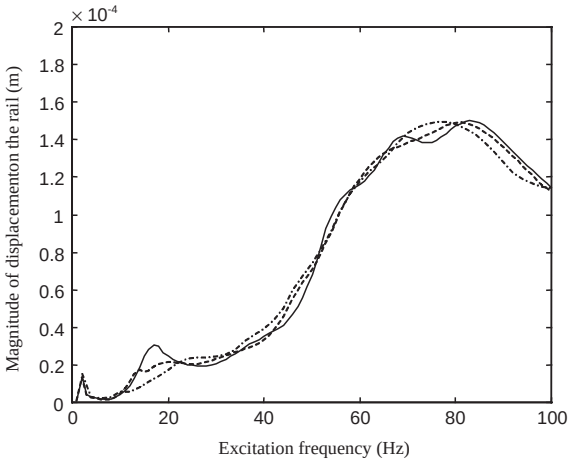

Fig. 4. Magnitude of the displacement of the wheel/rail contact point on the rail for the single-axle model plotted against frequency of excitation for irregularity of amplitude 0.1 mm. ——, for vehicle running at 0 m/s; – – –, for vehicle running at 30 m/s; – · –, for vehicle running at 60 m/s.

where $\omega_0 = \sqrt{k_1/M_C}$ denotes the natural frequency of the suspended mass on the suspension. From Eqs. (20) and (21),

$$\tilde{z}_{W1}(\Omega) = \frac{\sigma_{11}^T \tilde{z}_1(\Omega)}{(\sigma_{11}^T + \sigma_{11}^R + 1/k_{H1})}, \tag{38}$$

$$\tilde{z}_{R1}(\Omega) = -\frac{\sigma_{11}^R \tilde{z}_1(\Omega)}{(\sigma_{11}^T + \sigma_{11}^R + 1/k_{H1})}. \tag{39}$$

It can be seen from Eqs. (37)–(39) that, when $\Omega \to 0$, $\sigma_{11}^T \to \infty$, $\tilde{z}_{W1} \to \tilde{z}_1$, and $\tilde{z}_{R1} \to 0$. This low frequency feature is illustrated in Figs. 3 and 4. At the natural frequency of the suspended mass on the suspension (about 2 Hz), $\sigma_{11}^T = 0$ (if there is no damping), both the wheel–rail force and the displacement of the contact point on the rail have a peak while the displacement of the wheel has a local minimum.

For frequencies much higher than the natural frequency of the suspended mass on the suspension, the displacement of the suspended mass is negligible. Thus the receptance of the vehicle at the wheelset can be approximated by

$$\sigma_{11}^T = \frac{1}{(k_1 - M_W \Omega^2)} \tag{40}$$

which implies that, when $\Omega^2 = k_1/M_W$, i.e., around the natural frequency of the unsprung mass on the suspension (which is much higher than the natural frequency of the suspended mass on the suspension, since the unsprung mass is much smaller), $\sigma_{11}^T \to \infty$, $\tilde{P}_1 \to 0$, $\tilde{z}_{W1} \to \tilde{z}_1$, and $\tilde{z}_{R1} \to 0$. The presence of damping in the suspension of the vehicle produces a local minimum in the wheel–rail force and a local minimum in the rail displacement at this frequency. For the present vehicle parameters, this frequency is 9.2 Hz.

When $\Omega \to \infty$, then $\sigma_{11}^{T} \to 0$, $\sigma_{11}^{R} \to 0$, thus the wheel–rail force is bounded, as indicated by Eq. (36).

The effect of the layered structure of the ground is not apparent in the wheel–rail force whereas there is some effect on the displacements of the wheel–rail contact points. As shown in Fig. 4, for low vehicle speed, around the track-modified cut-on frequency of the ground system (16 Hz [6]), the displacement at the wheel–rail contact point on the rail has a peak and this peak is flattened when the vehicle speed increases.

Fig. 4 also shows that the vehicle speed does not have a significant effect on the displacement of the wheel–rail contact point on the rail. However, the vibration propagation in the track direction is strongly influenced by the vehicle travelling speed. To show this, the magnitudes of the vertical displacement along the x-axis on the ground surface for different excitation frequencies are shown in Figs. 5–7 for the three vehicle speeds. It can be seen that around the natural frequency of the suspended mass on the suspension (2 Hz), the ground surface has a peak response. Fig. 5 shows that when the excitation frequency is about 16 Hz, i.e., the track-modified cut-on frequency of the layered ground, strong vibration propagation occurs in the track direction. As the vehicle speed increases, this vibration propagation is greatly enhanced behind the vehicle and it has a broader frequency response. This can be seen by comparing Fig. 5 with Figs. 6 and 7.

5.1.2. *When the single axle runs on the heavier track on the ground*

Compared with the lighter track, the heavier track has more ballast mass and lower ballast stiffness. Some results for the heavier track on the ground and for high vehicle speed are shown in Figs. 8–11, with comparisons made with those for the lighter track.

Fig. 8 shows the magnitude of the wheel–rail force for the vehicle running at 60 m/s. It can be seen that for excitation frequencies lower than 67 Hz, the heavier track produces slightly less wheel–rail force than the lighter track. However, for higher excitation frequencies, the heavier track produces a much greater wheel–rail force. Fig. 9 shows the displacement of the wheelset plotted against excitation frequency and indicates that for excitation frequencies higher than

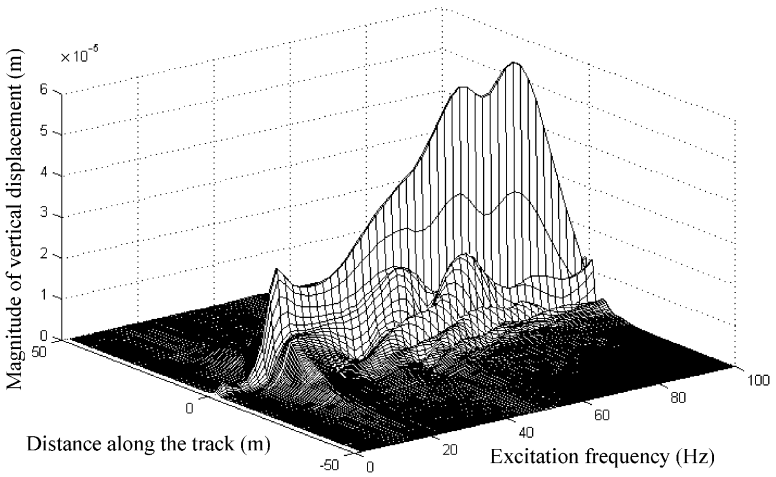

Fig. 5. Vertical displacement along the x-axis on the ground surface for $c = 0$ m/s for the single-axle model with irregularity of 0.1 mm.

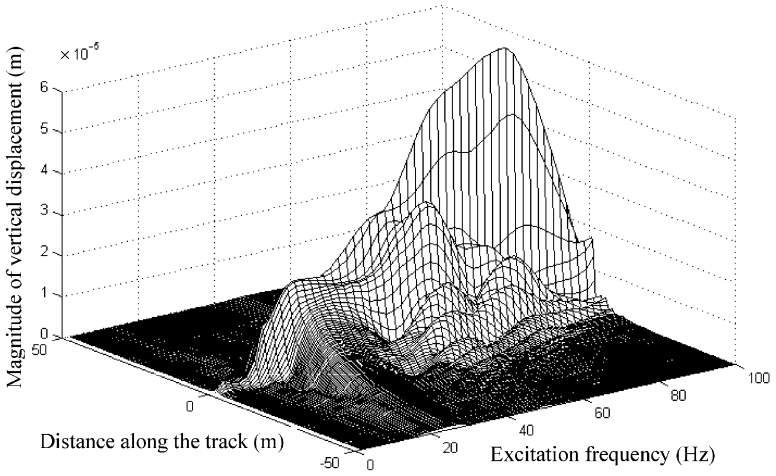

Fig. 6. Vertical displacement along the x-axis on the ground surface for $c = 30\,\mathrm{m/s}$ for the single-axle model with irregularity of 0.1 mm.

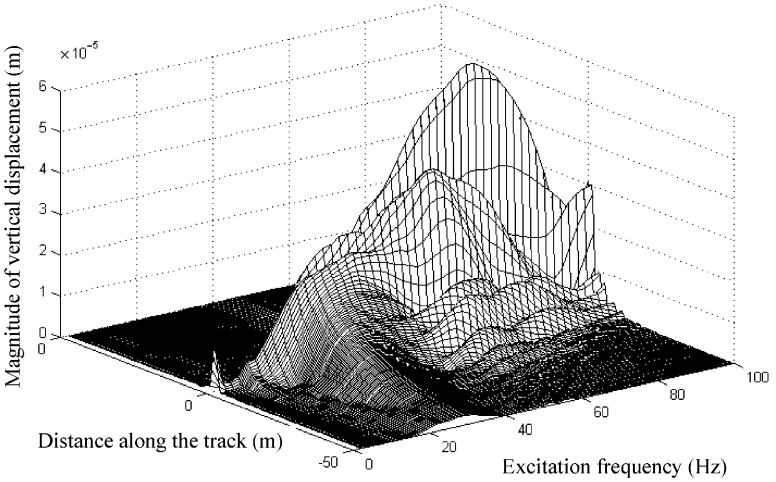

Fig. 7. Vertical displacement along the x-axis on the ground surface for $c = 60\,\mathrm{m/s}$ for the single-axle model with irregularity of 0.1 mm.

67 Hz, the displacement of the wheelset is greater when it runs on the heavier track. Figs. 10 and 11 present the maximum displacements along the rail and along the track centreline on the ground surface. Both these figures indicate that the heavier track produces less vibration for frequencies below 85 Hz. These example results illustrate the fact that the track structure can have an important influence on the vibration generated. The response along the track is strongly dependent on the speed of the vehicle even for speeds below the ground vibration propagation wave speeds.

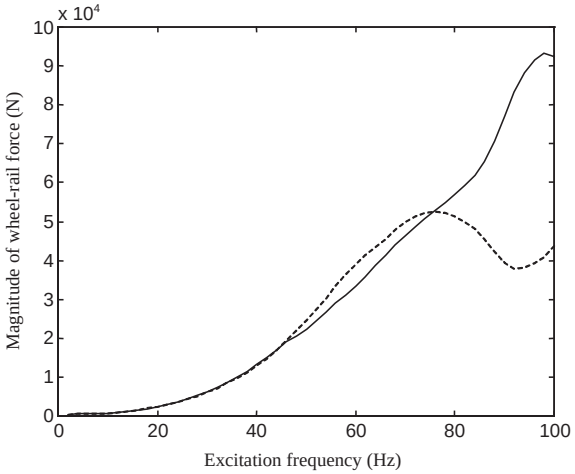

Fig. 8. Magnitude of the wheel–rail force plotted against excitation frequency for the vehicle running at 60 m/s. ——, for the single axle running on the heavier track; – – –, for the single axle on the lighter track.

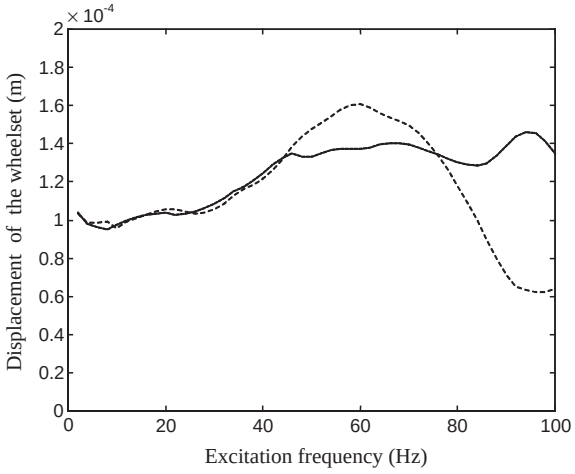

Fig. 9. Magnitude of the displacement of the wheelset plotted against excitation frequency for the vehicle running at 60 m/s. ——, for the single axle running on the heavier track; – – –, for the single axle on the lighter track.

5.2. Results for a Mk 3 passenger coach

In this section, the vertical velocity levels of the surface of the ground with different tracks are calculated using formula (33) for a single British Mk 3 passenger coach running at different speeds. The parameters for this vehicle are listed in Table 5. In addition to the two tracks (both are ballasted track) used in the last section, calculations are also performed for a slab track. The width and thickness of the slab are 2.5 and 0.25 m. Other parameters of the slab track are listed in Table 6. The slab track has almost the same mass as the heavier ballasted track. The difference

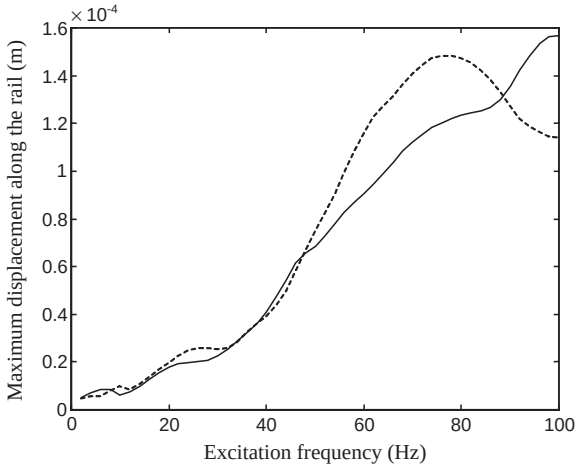

Fig. 10. Maximum displacement along the rails plotted against excitation frequency for the vehicle running at 60 m/s. ——, for the single axle running on the heavier track; – – –, for the single axle on the lighter track.

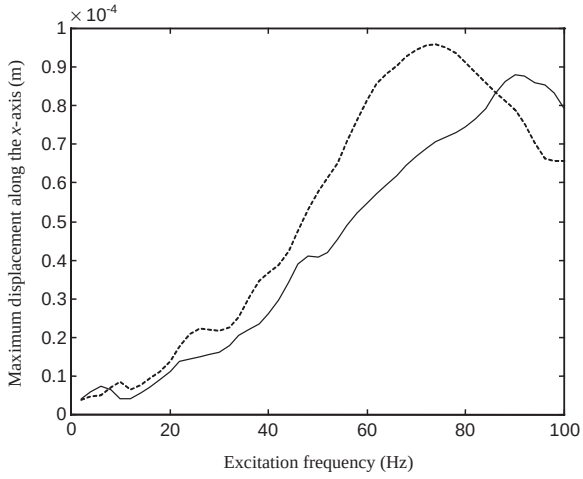

Fig. 11. Maximum displacement along the x-axis on the ground surface plotted against excitation frequency for the vehicle running at 60 m/s. ——, for the single axle running on the heavier track; – – –, for the single axle on the lighter track.

between the heavier track and the slab track is that the slab track has nearly ten times the bending stiffness and twice the vertical stiffness of the heavier track. For the analyses presented here, a vertical rail-head profile for nominally 'good' track measured on a 200 km/h mixed traffic main line in England is used in the calculation. For wavelengths from about 1.4 to 20 m (wave numbers from 0.7 to 0.05 cycles/m) this has been taken from track recording car data. This range of the data therefore corresponds to the loaded track profile albeit with the axle load of the track recording car rather than that of the vehicle for which the predictions are being made, although in this case the axle loads are similar. For shorter wavelengths, loaded profile data is not available.

Table 5
Parameters for the Mk 3 passenger coach

Mass of the car body (kg)	21,400
Pitch inertia moment of the car body (kg m^2)	8.3×10^5
Mass of each bogie (kg)	2707
Pitch inertia moment of each bogie (kg m^2)	1970
Secondary vertical stiffness per bogie (N/m)	0.81×10^6
Secondary vertical viscous damping (Ns/m)	74,000
Primary vertical stiffness per axle (N/m)	0.359×10^6
Primary vertical viscous damping per axle (Ns/m)	8400
Primary damper stiffness per axle	14×10^6
Distance between bogie centres (m)	2×8
Bogie wheelbase (m)	2×1.3
Mass of each wheelset (kg)	1375
Wheel diameter (m)	0.914

Table 6
Parameters for a slab track

Mass of rail beam per unit length of track	120 kg/m
Bending stiffness of rail beam	1.26×10^7 N m^2
Loss factor of the rail	0.01
Rail pad stiffness	2×10^8 N/m^2
Rail pad loss factor	0.25
Mass of slab per unit length of track	$(2.5 \times 0.25 \times 2400) = 1500$ kg/m
Bending stiffness of slab	1.11×10^8 N m^2
Loss factor of slab material	0.03
Contact width of track and ground	2.7 m

However, unloaded rail-head roughness measurements are made for the purposes of rolling noise studies [9] for vibration at higher frequency from trains in tunnels [13] and this has been found to overlap well with the track recording car data in the wavelength range from 1.4 to 20 m. This data has therefore been used to extend the roughness data to wavelengths down to 0.05 m (i.e., $\beta = 125$ rad/m). The wavelength range covered by the loaded measurement does not therefore include the wavelengths corresponding to the sleeper spacing at around 0.6 m. The combined one-third octave band spectrum for the track profile that has been used in the current work is shown in Fig. 12. Note that, since the same profile is assumed for each of the tracks, no effect is shown here of a possible improvement in track quality associated with a slab track compared to a ballasted track.

The predicted one-third octave vibration velocity spectra are presented here for three points on the ground surface and for three vehicle speeds, 25 m/s (90 km/h), 60 m/s (216 km/h) and 83 m/s (300 km/h). The distances from the three points to the track centreline are 5, 10 and 20 m. In order to indicate the roles of the quasi-static and dynamic mechanisms of excitation, the vertical velocity levels due to the quasi-static loads only are also shown.

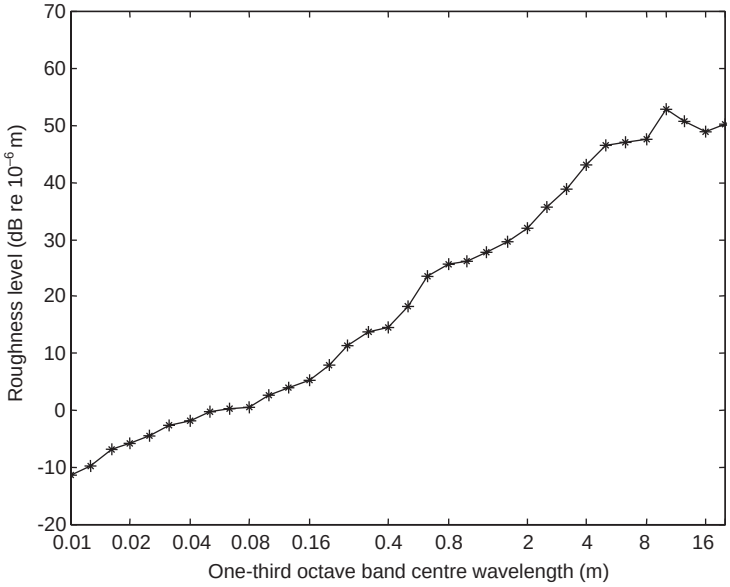

Fig. 12. One-third octave band spectrum of the vertical profile of the rails.

5.2.1. Levels observed at different distances from the track

Results are shown in Figs. 13–15 for the heavier track at three speeds. Three approximate frequency ranges may be identified in these figures: 1.6–6 Hz, 6–20 Hz and 20–80 Hz. These approximate ranges will be referred to as the *low*, *middle* and *upper* frequency ranges in this discussion. As seen in Figs. 13–15, the response level is dominated by the quasi-static loads for low frequencies. The lower the vehicle speed or the further the observer from the track, the more important is the dynamic component of excitation. For example, as shown in Fig. 14 for a vehicle speed of 60 m/s, the quasi-static loads are the dominant source for frequencies below 8 Hz at 5 m, 5 Hz at 10 m and 3.2 Hz at 20 m. In the *low* frequency range, which is dominated by the quasi-static loads, the attenuation rate with distance from the track is much greater than those in the *middle* and *upper* frequency ranges. In the *middle* frequency range, a strong rise in the total response level is observed around the track-modified cut-on frequency. In this frequency range, the vibration has smaller attenuation rate than in the *low* and the *upper* frequency ranges.

5.2.2. Effect of track structure on the response level

A comparison of the three tracks is presented in Figs. 16–18 for the three travelling speeds, 25, 60 and 83 m/s. In these figures only the velocity levels at 10 m on the ground surface are shown. Since the heavier ballasted track produces less ground vibration from the dynamic wheel–rail forces (see Fig. 11) but greater ground vibration from the quasi-static loads (see Ref. [6]) than the lighter track, the heavier track only gives a little reduction in vibration level in the *upper* frequency range. However, the slab track has quite a different behaviour. Due to its much greater bending stiffness, the slab track produces about 20 dB lower vibration level than either of the ballasted tracks for frequencies up to 25 Hz. Compared with the ballasted tracks, the slab track greatly reduces the vibration level due to the quasi-static loads, since the peak response load speed

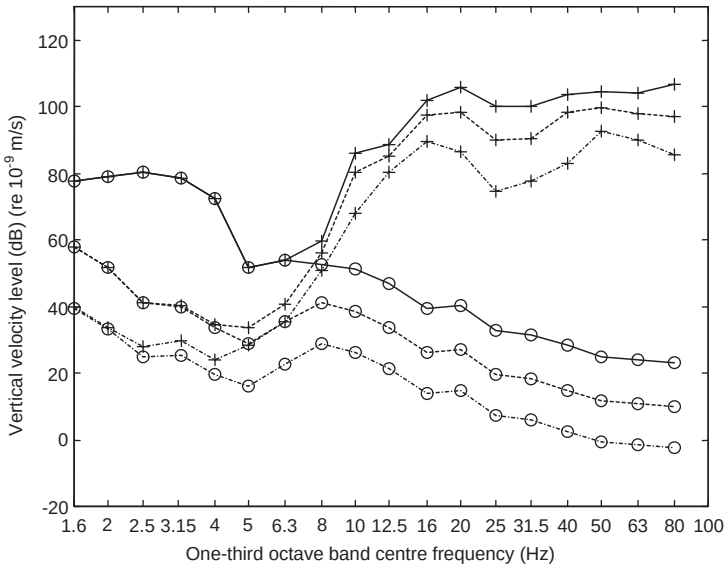

Fig. 13. Predicted vertical velocity levels for points at 5 m (——), 10 m (– – –) and 20 m (–·–) from the track centreline for a Mk 3 coach on the heavier track at 25 m/s. +: total level; ○: level due to the quasi-static loads.

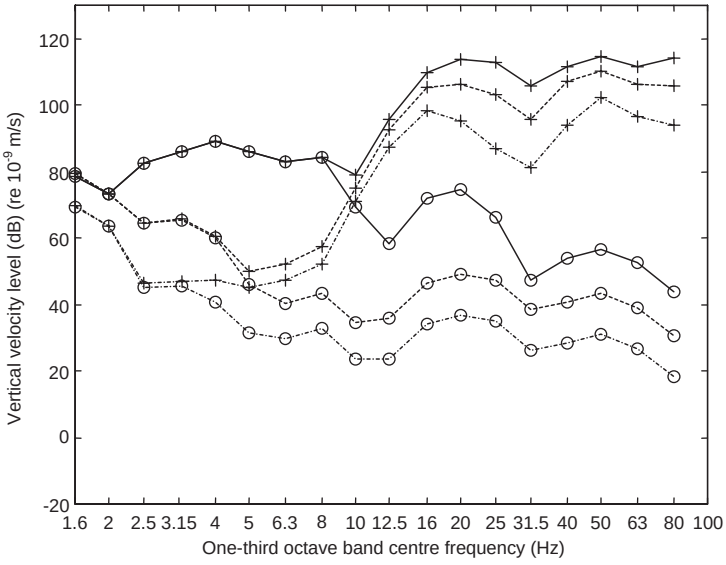

Fig. 14. Predicted vertical velocity levels for points at 5 m (——), 10 m (– – –) and 20 m (–·–) from the track centreline for a Mk 3 coach on the heavier track at 60 m/s. +: total level; ○: level due to the quasi-static loads.

(at which the ground has a maximum response) of the ground is significantly increased by the bending stiffness of the slab track; therefore it is more effective for low frequencies. For high frequencies, it may raise the level due to the increased dynamic wheel–rail forces. As can be seen, for frequencies higher than 40 Hz, the response levels for the three tracks are close to each other.

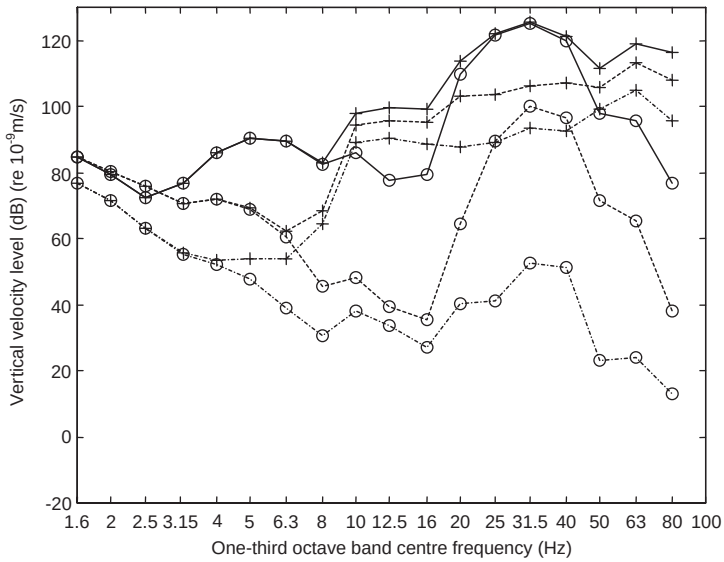

Fig. 15. Predicted vertical velocity levels for points at 5 m (——), 10 m (– – –) and 20 m (–·–) from the track centreline for a Mk 3 coach on the heavier track at 83 m/s. +: total level; ○: level due to the quasi-static loads.

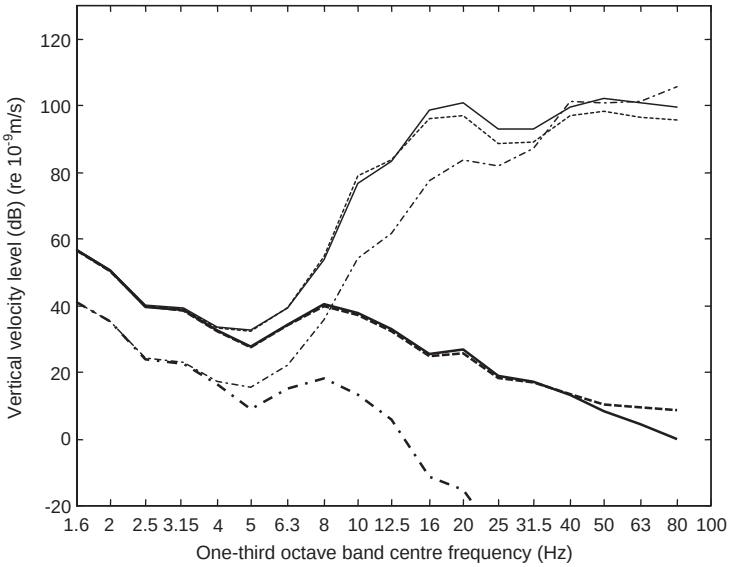

Fig. 16. Vertical velocity level at 10 m on the ground surface for vehicle speed 25 m/s. ——, for the lighter track; – – –, for the heavier track; –·–, for the slab track. Thicker lines are for the levels due to the quasi-static loads.

5.2.3. *Effect of vehicle speed on response level*

In Fig. 18, a strong rise in the vibration level due to the quasi-static loads is observed between 16 and 20 Hz. This is due to the direct excitation of propagating waves by the quasi-static loads moving at a speed (83 m/s) in excess of the lowest propagating wave speed (77 m/s) in the ground.

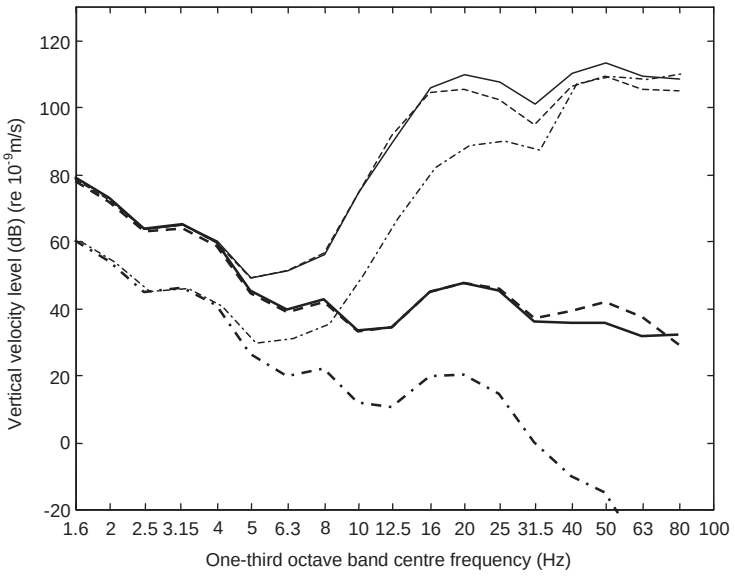

Fig. 17. Vertical velocity level at 10 m on the ground surface for vehicle speed 60 m/s. ——, for the lighter track; – – –, for the heavier track; –·–, for the slab track. Thicker lines are for the levels due to the quasi-static loads.

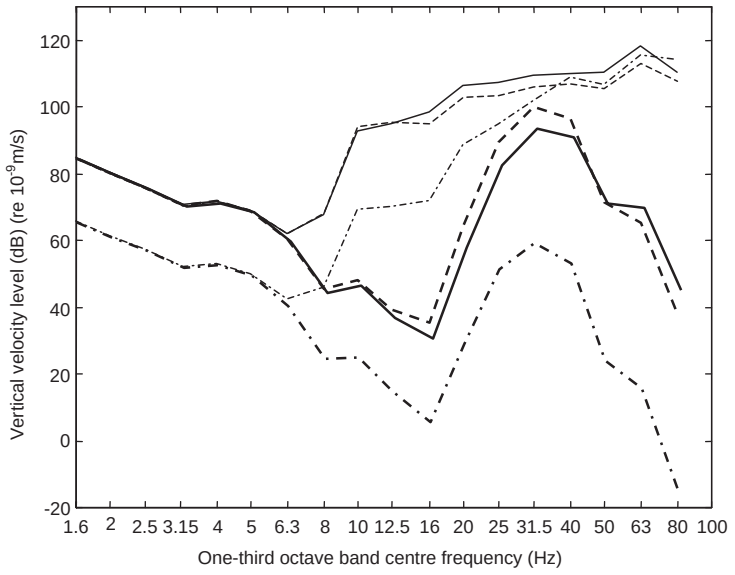

Fig. 18. Vertical velocity level at 10 m on the ground surface for vehicle speed 83 m/s. ——, for the lighter track; – – –, for the heavier track; –·–, for the slab track. Thicker lines are for the levels due to the quasi-static loads.

The results at different vehicle travelling speeds for the heavier track are compared in Fig. 19 for a point at 10 m on the ground surface. As the vehicle speed increases, the upper limit of frequency at which the quasi-static loads are the dominant source is slightly increased, from 3.2 Hz for 25 m/s to 6 Hz for 83 m/s. Since the quasi-static loads are the dominant mechanism of excitation only for

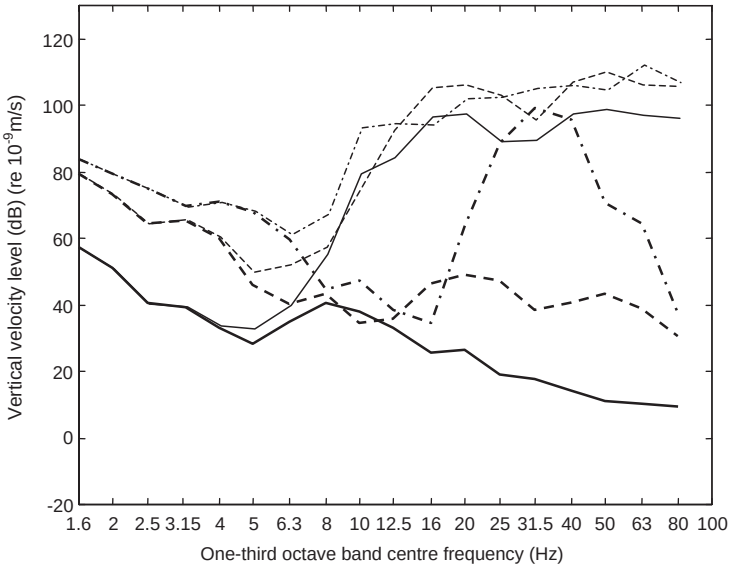

Fig. 19. Vertical velocity level at 10 m on the ground surface with the heavier track for different vehicle speeds. ——, 25 m/s; – – –, 60 m/s; –·–, 83 m/s. Thicker lines are for the levels due to the quasi-static loads.

frequencies below the track–ground system cut-on frequency, the vehicle speed has a greater effect on the response level for this low frequency range. For higher frequencies, though the response level due to the quasi-static loads is strongly dependent on the vehicle speed, the dynamic response and, therefore the total response level, is far less dependent on this. This may be roughly explained using Fig. 2 which shows that for a large range of frequency, the vehicle speed has little effect on the dynamic wheel–rail forces apart from changes as the rail profile spectrum shifts to higher frequencies.

The features revealed here by considering a single coach are confirmed by the measurements at three sites [5]. These sites present different ground conditions (very soft, fairly soft and hard) and different train-traffic operations (high-speed passenger trains and low-speed freight trains of two-axle wagons). For instance, the excitation of the propagating mode has been observed in the site with the very soft ground when passenger trains travel at speeds higher than the lowest ground wave speed. A strong rise in the total response level around the track-modified cut-on frequency has been validated at the site with the hard ground. A separate paper [5] that is now in preparation will describe the prediction and comparison between the model and the measured data at the three sites.

6. Conclusions

In the present paper, the vertical dynamics of vehicles running at constant speed on a track are coupled with the track–ground model developed in Ref. [6], producing a complete ground vibration model incorporating vehicles, track and ground. A relationship is derived between the vertical rail irregularity spectral density and the ground vibration power spectra. This relationship

means that predictions from the model can be presented in terms comparable to actual vibration measurements.

From this model, the wheel–rail dynamic force and the maximum displacement along the track centreline on the ground surface are calculated for a single-axle vehicle model and for two different ballasted tracks. It is shown that, for a large range of frequency, the layered structure of the ground and the vehicle speed have little effect on the dynamic wheel–rail force and the displacements of the wheel–rail contact points. However, wave propagation in the track direction is strongly enhanced by the motion of the vehicle. The track parameters have a significant effect on the vibration due to the dynamic wheel–rail force.

The vertical velocity levels of the surface of a typical soft ground are also produced from this model for a single Mk 3 passenger coach running on the ballasted tracks and a slab track. Three frequency ranges are identified by these results: frequencies much below the cut-on frequency of the track–ground system (*low* frequency range), frequencies around the cut-on frequency (*middle* frequency range) and frequencies above this (*upper* frequency range). Only in the *low* frequency range is the response level dominated by the quasi-static loads. The lower the vehicle speed or the further the observer from the track, the more important is the dynamic component of excitation compared to the quasi-static loads. In the *low* frequency range, the rate of attenuation with distance from the track is much higher than those in the other two frequency ranges. In the *middle* frequency range, a strong rise in the total response level is observed due to the cut-on of a propagating wave mode in the track–ground system. In this frequency range, the vibration has a smaller attenuation rate than in the *low* and the *upper* frequency ranges.

Compared with the lighter ballasted track, the heavier track only gives a little reduction in vibration level in the *upper* frequency range. The slab track produces about 20 dB lower vibration level at 10 m than either of the ballasted tracks for frequencies up to 25 Hz due to its much higher bending stiffness. Compared with the ballasted tracks, the slab track greatly reduces the vibration level due to the quasi-static loads, since the peak response load speed of the ground with the slab track is significantly increased by the bending stiffness of the track; it is therefore more effective for low frequencies. For high frequencies, it may increase the observed vibration level due to the increased dynamic wheel–rail forces.

The upper limit of frequency for which the quasi-static loads are the dominant source is increased slightly with increasing vehicle speed. Since the quasi-static loads are the dominant mechanism of excitation for frequencies below the cut-on frequency, the vehicle travelling speed has a greater effect on the response level for this frequency range. For higher frequencies, although the response level due to the quasi-static loads is greatly dependent on the vehicle speed, the total response level is not so sensitive to the speed.

Appendix A. The mass and stiffness matrices of vehicles

In this appendix, the mass and stiffness matrices are derived for vehicles of three types. The mass and the pitch inertia of the car body are denoted by M_C and J_C. The vertical displacement and the pitch angle of the car body are denoted by $z_c(t)$ and $\varphi_c(t)$. The mass and the pitch inertia of each bogie are denoted by M_B and J_B. The vertical displacement and the pitch angle of the jth bogie are denoted by $z_{Bj}(t)$ and $\varphi_{Bj}(t)$. The mass of each wheelset is denoted by M_W, and the

vertical displacement of the lth wheelset is denoted by $z_{Wl}(t)$. For the vertical displacements, the positive direction is downwards, while for the pitch angles, the positive direction is clockwise. The (complex) stiffness of a primary suspension (between wheelset and bogie) per axle is denoted by k_1, and that of a secondary suspension (between bogie and car body) per bogie is denoted by k_2. For different types of suspension, k_1 and k_2 are different functions of frequency, stiffness and damping of the suspension. When a suspension, for example a primary suspension, consists of a spring and a viscous damper which are connected in parallel, as shown in Fig. 20a, then

$$k_1 = k_{S1} + \mathrm{i}\Omega c_{S1}, \tag{A.1}$$

where k_{S1} denotes the stiffness of the spring, c_{S1} the viscous damping coefficient of the damper and Ω the angular frequency. If the suspension has a structure shown in Fig. 20b, in which an extra spring is connected in series with the damper, then

$$k_1 = \frac{k_{S1}k'_{S1} + \mathrm{i}\Omega c_{S1}(k_{S1} + k'_{S1})}{(k'_{S1} + \mathrm{i}\Omega c_{S1})}. \tag{A.2}$$

Hysteretic damping can be incorporated into the suspension by introducing complex spring stiffness. A symbol, shown in Fig. 20c, is used to represent a suspension of any type.

A.1. For vehicle type I

Vehicle type I, shown in Fig. 21, represents a passenger coach with both a primary and a secondary suspension. The displacement vector of the vehicle is defined as

$$\{\mathbf{z}_V(t)\} = (z_C(t), \varphi_C(t), z_{B1}(t), \varphi_{B1}(t), z_{B2}(t), \varphi_{B2}(t), z_{W1}(t), z_{W2}(t), z_{W3}(t), z_{W4}(t))^{\mathrm{T}}. \tag{A.3}$$

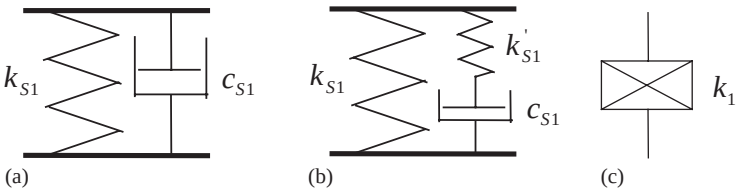

Fig. 20. Structure of suspensions.

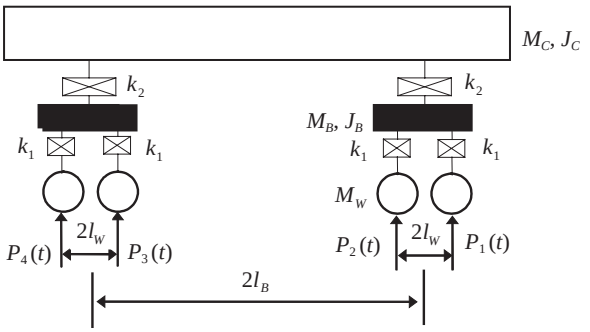

Fig. 21. Vehicle type I: a vehicle system with primary and secondary suspensions.

Corresponding to this displacement vector, the external force vector is determined as (refer to Eq. (1))

$$\{\mathbf{F}_V(t)\} = (0,0,0,0,0,0,-P_1(t),-P_2(t),-P_3(t),-P_4(t))^{\mathrm{T}} = -[\mathbf{B}]\{\mathbf{P}(t)\}, \tag{A.4}$$

where

$$[\mathbf{B}] = \begin{bmatrix} [\mathbf{0}]_{6\times4} \\ [\mathbf{I}]_{4\times4} \end{bmatrix} \tag{A.5}$$

and

$$\{\mathbf{P}(t)\} = (P_1(t), P_2(t), P_3(t), P_4(t))^{\mathrm{T}} \tag{A.6}$$

is the vertical wheel–rail force vector.

The wheelset displacement vector can be written as (see Eq. (8))

$$\{\mathbf{z}_W(t)\} = [\mathbf{A}]\{\mathbf{z}_V(t)\}, \tag{A.7}$$

where

$$[\mathbf{A}] = [[\mathbf{0}]_{4\times6}\ [\mathbf{I}]_{4\times4}] = [\mathbf{B}]^{\mathrm{T}}. \tag{A.8}$$

The mass matrix is given by

$$[\mathbf{M}_V] = \mathrm{diag}(M_C, J_C, M_B, J_B, M_B, J_B, M_W, M_W, M_W, M_W) \tag{A.9}$$

the stiffness matrix by

$$[\mathbf{K}_V] = \begin{bmatrix}
2k_2 & 0 & -k_2 & 0 & -k_2 & 0 & 0 & 0 & 0 & 0 \\
0 & 2k_2l_B^2 & -k_2l_B & 0 & k_2l_B & 0 & 0 & 0 & 0 & 0 \\
-k_2 & -k_2l_B & k_2+2k_1 & 0 & 0 & 0 & -k_1 & -k_1 & 0 & 0 \\
0 & 0 & 0 & 2k_1l_W^2 & 0 & 0 & -k_1l_W & k_1l_W & 0 & 0 \\
-k_2 & k_2l_B & 0 & 0 & k_2+2k_1 & 0 & 0 & 0 & -k_1 & -k_1 \\
0 & 0 & 0 & 0 & 0 & 2k_1l_W^2 & 0 & 0 & -k_1l_W & k_1l_W \\
0 & 0 & -k_1 & -k_1l_W & 0 & 0 & k_1 & 0 & 0 & 0 \\
0 & 0 & -k_1 & k_1l_W & 0 & 0 & 0 & k_1 & 0 & 0 \\
0 & 0 & 0 & 0 & -k_1 & -k_1l_W & 0 & 0 & k_1 & 0 \\
0 & 0 & 0 & 0 & -k_1 & k_1l_W & 0 & 0 & 0 & k_1
\end{bmatrix} \tag{A.10}$$

A.2. For vehicle type II

Fig. 22 (vehicle type II) shows a freight vehicle with only one level of suspension which is installed between the car body and the bogies. The displacement vector is defined as

$$\{\mathbf{z}_V(t)\} = (z_C(t), \varphi_C(t), z_{B1}(t), \varphi_{B1}(t), z_{B2}(t), \varphi_{B2}(t))^{\mathrm{T}}. \tag{A.11}$$

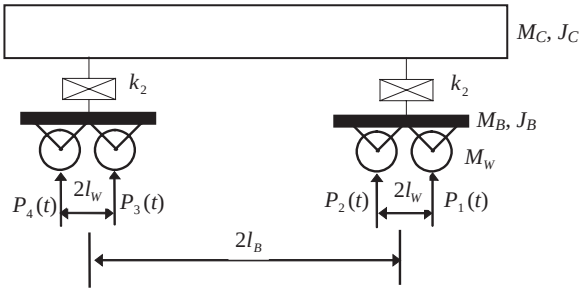

Fig. 22. Vehicle type II: a vehicle system with only secondary suspensions.

Thus the external force vector is determined by

$$\{\mathbf{F}_V(t)\} = -[\mathbf{B}]\{\mathbf{P}(t)\}, \tag{A.12}$$

where

$$[\mathbf{B}] = \begin{bmatrix} 0 & 0 & 0 & 0 \\ 0 & 0 & 0 & 0 \\ 1 & 1 & 0 & 0 \\ l_W & -l_W & 0 & 0 \\ 0 & 0 & 1 & 1 \\ 0 & 0 & l_W & -l_W \end{bmatrix}. \tag{A.13}$$

The wheelset displacement vector is given by

$$\{\mathbf{z}_W(t)\} = [\mathbf{A}]\{\mathbf{z}_V(t)\}, \tag{A.14}$$

where

$$[\mathbf{A}] = \begin{bmatrix} 0 & 0 & 1 & l_W & 0 & 0 \\ 0 & 0 & 1 & -l_W & 0 & 0 \\ 0 & 0 & 0 & 0 & 1 & l_W \\ 0 & 0 & 0 & 0 & 1 & -l_W \end{bmatrix} = [\mathbf{B}]^{\mathrm{T}}. \tag{A.15}$$

The mass matrix is given by

$$[\mathbf{M}_V] = diag(M_C, J_C, M_B + 2M_W, J_B + 2M_W l_W^2, M_B + 2M_W, J_B + 2M_W l_W^2) \tag{A.16}$$

and the stiffness matrix by

$$[\mathbf{K}_V] = \begin{bmatrix} 2k_2 & 0 & -k_2 & 0 & -k_2 & 0 \\ 0 & 2k_2 l_B^2 & -k_2 l_B & 0 & k_2 l_B & 0 \\ -k_2 & -k_2 l_B & k_2 & 0 & 0 & 0 \\ 0 & 0 & 0 & 0 & 0 & 0 \\ -k_2 & k_2 l_B & 0 & 0 & k_2 & 0 \\ 0 & 0 & 0 & 0 & 0 & 0 \end{bmatrix} \tag{A.17}$$

A.3. For vehicle type III

Fig. 23 (vehicle type III) shows a freight vehicle with two axles. The displacement vector is defined as

$$\{\mathbf{z}_V(t)\} = (z_C(t), \varphi_C(t), z_{W1}(t), z_{W2}(t))^{\mathrm{T}}. \tag{A.18}$$

Thus the external force vector is determined by

$$\{\mathbf{F}_V(t)\} = -[\mathbf{B}]\{\mathbf{P}(t)\}, \tag{A.19}$$

where

$$[\mathbf{B}] = \begin{bmatrix} 0 & 0 \\ 0 & 0 \\ 1 & 0 \\ 0 & 1 \end{bmatrix}. \tag{A.20}$$

The wheelset displacement vector is given by

$$\{\mathbf{z}_W(t)\} = [\mathbf{A}]\{\mathbf{z}_V(t)\}, \tag{A.21}$$

where

$$[\mathbf{A}] = \begin{bmatrix} 0 & 0 & 1 & 0 \\ 0 & 0 & 0 & 1 \end{bmatrix} = [\mathbf{B}]^{\mathrm{T}}. \tag{A.22}$$

The mass matrix is given by

$$[\mathbf{M}_V] = \mathrm{diag}(M_C, J_C, M_W, M_W) \tag{A.23}$$

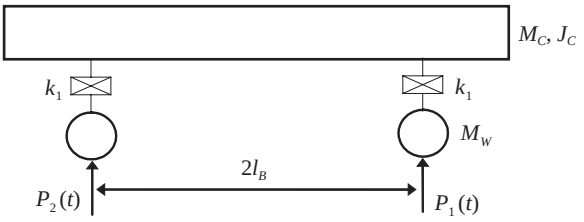

Fig. 23. Vehicle type III: a two-axle vehicle.

and the stiffness matrix by

$$[\mathbf{K}_V] = \begin{bmatrix} 2k_1 & 0 & -k_1 & -k_1 \\ 0 & 2k_1 l_B^2 & -k_1 l_B & k_1 l_B \\ -k_1 & -k_1 l_B & k_1 & 0 \\ -k_1 & k_1 l_B & 0 & k_1 \end{bmatrix}. \tag{A.24}$$

References

[1] H. Takemiya, *Ground vibrations alongside track induced by high-speed trains: prediction and mitigation*, in: V.V. Krylov (Ed.), Noise and Vibration from High-speed Trains, Thomas Telford, London, 2001, pp. 347–393.

[2] V.V. Krylov, Calculation of low frequency vibrations from railway trains, *Applied Acoustics* 42 (1994) 199–213.

[3] H. Grundmann, M. Lieb, E. Trommer, The response of a layered half-space to traffic loads moving along its surface, *Archive of Applied Mechanics* 69 (1) (1999) 55–67.

[4] C.G. Lai, A. Callerio, E. Faccioli, A. Martino, Mathematical modelling of railway-induced ground vibrations, *Proceedings of the International Workshop Wave 2000*, Bochum, Germany, 2000, 99–110.

[5] X. Sheng, C.J.C. Jones, D.J. Thompson, A comparison of a theoretical model for quasi-statically and dynamically induced environmental vibration from trains with measurements, *Journal of Sound and Vibration* 267 (3) (2003) 621–635.

[6] X. Sheng, C.J.C. Jones, M. Petyt, Ground vibration generated by a load moving along a railway track, *Journal of Sound and Vibration* 228 (1) (1999) 129–156.

[7] W. Zai, *Dynamics of Coupled Vehicle-Track Systems*, China Railway Press, Beijing, 1997, pp. 30–32 (In Chinese).

[8] ORE C116, 1971 C116/RP1, Power spectral density of track irregularities, Part 1: definitions, conventions and available data.

[9] P.C. Dings, M.G. Dittrich, Roughness on Dutch railway wheels and rails, *Journal of Sound and Vibration* 193 (1) (1996) 103–112.

[10] C. Esveld, Modern Railway Track, MRT Productions, Duisburg, Germany, 1989, pp. 314–315.

[11] H.H. Jenkins, J.E. Stephenson, G.A. Clayton, G.W. Morland, D. Lyon, The effect of track and vehicle parameters on wheel/rail vertical dynamic forces, *Railway Engineering Journal* 3 (1) (1974) 2–16.

[12] X. Sheng, C.J.C. Jones, D.J. Thompson, A theoretical study on the influence of the track on train-induced ground vibration, *Journal of Sound and Vibration* 272 (3–5) (2004) 909–936, this issue.

[13] C.J.C. Jones, Reduction of noise and ground vibration from freight trains, *Selected Papers Presented at S-Tech—A Conference on Railway Speed-up Technology, Institute of Mechanical Engineering Conference Transactions 1996–8,* Birmingham, 1996, pp. 87–97.